Analyzing the distribution of progression-free survival for combination therapies: A study of model-based translational predictive methods in

European Journal of Pharmaceutical Sciences 203 (2024) 106901

Contents lists available at ScienceDirect

European Journal of Pharmaceutical Sciences

journal homepage: www.elsevier.com/locate/ejps

Analyzing the distribution of progression-free survival for combination therapies: A study of model-based translational predictive methods in oncology

Marcus Baaz [a,b,*], Tim Cardilin [a], Mats Jirstrand [a]

[a] Fraunhofer-Chalmers Research Centre for Industrial Mathematics, Gothenburg, Sweden
[b] Department of Mathematical Sciences, Chalmers University of Technology and University of Gothenburg, Gothenburg, Sweden

ARTICLE INFO

Keywords:
Progression-free survival
Combination therapy
Oncology
Nonlinear mixed effects

ABSTRACT

Progression-free survival (PFS) is an important clinical metric in oncology and is typically illustrated and evaluated using a survival function. The survival function is often estimated *post-hoc* using the Kaplan-Meier estimator but more sophisticated techniques, such as population modeling using the nonlinear mixed-effects framework, also exist and are used for predictions. However, depending on the choice of population model PFS will follow different distributions both quantitatively and qualitatively. Hence the choice of model will also affect the predictions of the survival curves.

In this paper, we analyze the distribution of PFS for a frequently used tumor growth inhibition model with and without drug-resistance and highlight the translational implications of this. Moreover, we explore and compare how the PFS distribution for combination therapy differs under the hypotheses of additive and independent-drug action.

Furthermore, we calibrate the model to preclinical data and use a previously calibrated clinical model to show that our analytical conclusions are applicable to real-world setting. Finally, we demonstrate that independent-drug action can effectively describe the tumor dynamics of patient-derived xenografts (PDXs) given certain drug combinations.

1. Introduction

Combination therapies are a fundamental part of modern anti-cancer treatments and two often cited reasons for their effectiveness are the ability to mitigate drug resistance and the potential to induce synergistic effects (Mokhtari et al., 2017; Fitzgerald et al., 2006; Vakil and Trappe, 2019). However, it has been shown that synergy is not a requirement for a successful combination therapy (Palmer and Sorger; 2017). The independent drug action model, which assumes that the expected response of a patient given a combination therapy is the best response to the individual drugs, together with sufficient inter-patient variability is often able to account for the therapeutic benefits of combination therapy (Plana et al., 2022; Pomeroy et al., 2022).

Drug development is a long and complex process that begins on the molecular level and hopefully ends successfully after several clinical trials (Mohs and Greig, 2017). Along the development process, there are many pitfalls, including particularly challenging translational steps from one phase to the next, *e.g.,* from *in vitro* to *in vivo* or from preclinical to clinical (Mak et al., 2014; Seyhan, 2019). Only about 15 % of drugs that enter clinical trials gain regulatory approval (Arrowsmith and Miller, 2013). This highlights the need to better understand the disease condition as well as the translational challenges faced throughout the drug development process.

Patient-derived xenografts (PDXs) play an important role in the early evaluation of new anti-cancer drugs (Koga and Ochiai, 2019). Tumor growth inhibition (TGI), is a metric estimated by comparing the tumor size of untreated and treated PDXs at a specific time point and is used to rank test compounds and decide which should be selected for continued development (Wu, 2010). However, attempts have also been made to facilitate translation into the clinic by estimating or predicting clinically relevant metrics such as overall response rate (the proportion of patients achieving a partial or complete response to the treatment) and progression-free survival (PFS) directly from PDXs (Gao et al., 2015; Wong et al., 2012; Baaz et al., 2022). The response evaluation criteria for

* Corresponding author at: Fraunhofer-Chalmers Centre, Chalmers Science Park, Gothenburg, 412 88, Sweden.
E-mail address: Marcus.Baaz@fcc.chalmers.se (M. Baaz).

https://doi.org/10.1016/j.ejps.2024.106901
Received 20 February 2024; Received in revised form 12 August 2024; Accepted 9 September 2024
Available online 10 September 2024

solid tumors (RECIST) is a framework for how to report and compare clinical studies in oncology and PFS is the time until tumor progression (or death), defined in RECIST (Gutman et al., 2013; Eisenhauer et al., 2009). PFS is a clinical efficacy metric on its own but also serves as a surrogate for overall survival - the gold standard for comparing treatments in oncology (Zhuang et al., 2009). To adequately translate PFS across species, differences in disease conditions between mice and humans, and the structures of preclinical and clinical trials, must be accounted for.

Mathematical modeling is an important part of modern drug discovery (Slater et al., 2017). Models are developed to capture tumor size dynamics, which in turn can be used to predict response rates and PFS (Claret et al., 2009). Using simulations, complex models can be evaluated and used to inform decision-making. However, with increased model complexity comes the problem of understanding the qualitative nature of the model, which can have essential biological and translational implications. This can potentially be solved by analytically investigating a simpler version of the model to gain qualitative knowledge and then extending it to the more complex model through computer simulations.

With this paper, we have three aims. First, to investigate how the PFS time is distributed for a commonly used preclinical and a clinical model, respectively. From this, we aim to show that there are quantitative as well as qualitative differences that have to be taken into consideration when performing translational predictions. To illustrate these results, we calibrate the models to preclinical PDX data and compare the derived distribution of PFS with that of a previously developed clinical model (Baaz et al., 2023). The second aim is to analyze PFS under two alternative combination therapy hypotheses: additive efficacy and independent-drug action. Lastly, building on research that suggests that the superiority of many combination therapies over their monotherapy counterparts can be attributed to the independent drug action hypothesis (Palmer and Sorger, 2017; Plana et al., 2022; Pomeroy et al., 2022), we investigate if the same hypothesis can be used in dynamical system modeling.

2. Methods

We first present the tumor dynamics model that we later both analyze analytically and calibrate to experimental data. The data we use is then detailed in the next subsection. Next, the necessary knowledge regarding PFS for the analysis is presented and the final subsection is focused on the computational methods used for the parameter estimation.

2.1. Model structure

2.1.1. Tumor dynamics

We consider a mathematical model describing the dynamics of tumor size (TS) following combination therapy with two anti-cancer agents, given in Eq (1).

$$\begin{aligned} &\frac{dTS(t)}{dt} = \big(k_g - G(k_1(t), k_2(t), p)\big)TS(t), TS(0) = TS_0, \\ &k_i(t) = \alpha_i C_i(t) e^{-\gamma_i t}, i = 1, 2. \end{aligned} \tag{1}$$

In Eq. (1), k_g denotes the tumor growth rate, which is assumed to be exponential in the absence of treatment, and TS_0 denotes the initial tumor size. The function k_i corresponds to cell killing induced by anti-cancer agent i, with concentration C_i, drug potency parameter α_i, and resistance γ_i, according to the Claret model (Claret et al., 2009). The function G is introduced to describe the net cell killing during combination treatment with the two drugs and is given by,

$$G(x, y, p) := (x^p + y^p)^{\frac{1}{p}}$$

for all real $x, y > 0$ and $p > 0$. In this way, the parameter p regulates the nature of the interaction between the two drugs, with $p = 1$ corresponding to additivity, $p < 1$ synergy, and $p > 1$ antagonism. Additionally, independent drug action is also covered using this formula, since,

$$(x^p + y^p)^{\frac{1}{p}} \to \max(x, y), \ as \ p \to +\infty.$$

Note that for $p \geq 1$, this is the standard p-norm. Mohamed et al. presented a similar approach for modeling combination therapy efficacy (Mohamed et al., 2016).

To make the subsequent analysis tractable, we shall frequently approximate the drug concentration $C_i(t)$ with the average concentration, $\overline{C_i}$. The analysis can also be performed using complete pharmacokinetic (PK) models, but this is more suitable for a simulation-based analysis since the resulting analytical expressions are dependent on the particular choice of PK model and quickly become intractable.

The left part of Fig. 1 shows the average concentrations resulting in $G = 1$ at $t = 0$ for different values of p.

2.1.2. Population variability

An important aspect that must be considered when using this type of model to describe population data is how to quantify the variability in the data. A popular method for this is the nonlinear mixed effects (NLME) framework, where a set of model parameters are assumed to follow a distribution in the population (Leander et al., 2021). The lognormal distribution is one of the most used distributions in population modeling and $X \sim LN(\mu, \sigma)$ if $\log(X) \sim N(\mu, \sigma)$, where μ and σ are the mean and standard deviation of the normal distribution, respectively. Here and throughout the paper log refers to the natural logarithm. For more information regarding the lognormal distribution, see the supplementary information.

The right part of Fig. 1 illustrates the required average concentration of the two drugs for the median individual of a large population to have $G = 1$ at $t = 0$ for different values of p. Here we have assumed independent and lognormally distributed normalized kill rates, *i.e.,* $a_i \sim LN(0, 1), \ i = 1, 2,$ and the median plots are obtained through Monte Carlo simulations.

The curve ($p = 10$) in the left part of Fig. 1 gives the impression that increasing the average concentration of drug 1 gives no benefit, under independent-drug action, up until a certain point. Although this is true when considering a single individual, it is, as seen in the right part of the figure, not the case on a population level.

2.1.3. Progression-free survival

According to the RECIST (version 1.1) guidelines, tumor lesions are classified as either target or non-target lesions (Eisenhauer et al., 2009). Target lesions are quantitatively measured during the trial, whereas non-target lesions are only monitored qualitatively.

PFS is determined by either target progression (TP) or non-target progression (*e.g.,* appearance of additional lesions). However, in this analysis, we will assume that PFS is determined by TP solely. TP occurs if the tumor size, TS, in terms of SLD for human patients, has increased by 20 % and 5 mm compared to the nadir TS. We only consider the percentage condition. How much the tumor has grown or shrunk (in %) at time t from the nadir is calculated according to,

$$100 \ \frac{TS(t) - TS_{nadir}}{TS_{nadir}},$$

and the time for PFS (target progression), T, is found by solving,

$$20 = 100 \ \frac{TS(T) - TS_{nadir}}{TS_{nadir}}. \tag{2}$$

PFS is often described using a survival function, $S(t)$, defined as the probability that the PFS event occurs after time t, *i.e.,* $S(t) = \Pr(T > t) =$

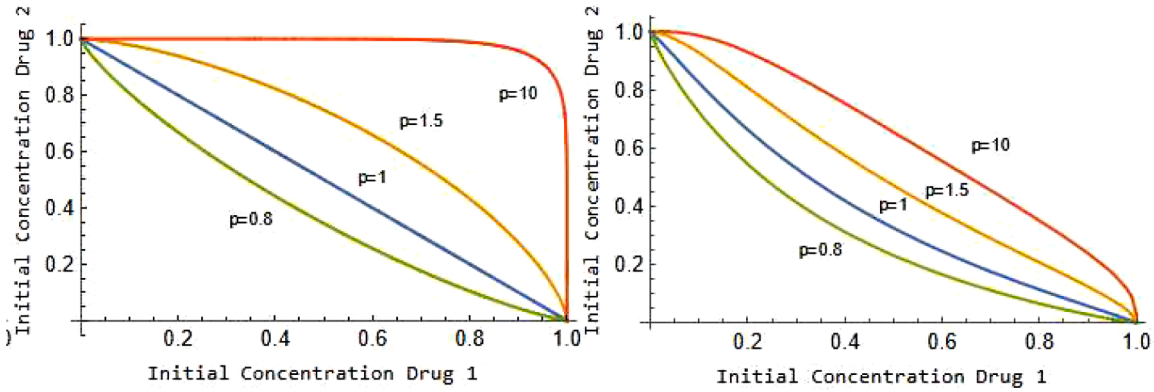

Fig. 1. (Left) Average concentrations resulting in $G = 1$ at $t = 0$ for different values of p. (Right) Average concentrations resulting in $G = 1$ at $t = 0$ for the median individual for different values of p.

$1 - F_T(t)$. Here $F_T(t)$ is the cumulative distribution function (CDF) of T. The probability density function (PDF) of T is denoted by f_T.

We derive the CDF of the PFS time for patients given both monotherapy and combination therapy. In the combination therapy case, we consider additive ($p = 1$), synergistic/antagonistic ($p \neq 1$) combination therapies as well as independent drug action ($p \to +\infty$) with and without correlation. Both the case of negligible ($\gamma_1 = \gamma_2 = 0$), and non-negligible resistance are considered and in the latter case, we consider the assumption of equal ($\gamma_1 = \gamma_2$), and different rates ($\gamma_1 \neq \gamma_2$), of acquired drug resistance.

In a previous paper (Baaz et al., 2023), we calibrated a joint model, for predicting PFS for clinical studies, with data coming from the PRIME study (Douillard et al., 2013). The study evaluated FOLFOX4 against FOLFOX4 + Panitumumab for metastatic colorectal cancer (mCRC) patients. The joint model consists of a TGI model and a time-to-event model. The TGI model was specified by, Eq. (1) as an additive combination therapy ($p = 1$) with equal rate of acquired resistance ($\gamma_1 = \gamma_2 \neq 0$), and was used to quantify when patients had a PFS event due to target progression. In this paper, we make simulations with this model by generating sets of individual parameters, which can be thought of as sets of virtual patients. These patients are given the combination therapy and their estimated PFS times show how PFS is distributed under a clinically relevant model. The data from the PRIME study was not further analyzed in this paper.

2.2. Modeling of preclinical data

Gao et al. have published a dataset of PDX trials, where the PDXs were created from many different patients, with several replicates for each patient, and used to test the efficacy of a large number of drugs (Gao et al., 2015). We use Eq. (1), to model a selected subset of these data, see Table 1. Since these data do not show clear signs of resistance formation, which other researchers have also concluded (Douillard et al., 2013), we simplify the model for preclinical data by setting $\gamma_i = 0$. The length (few significantly longer outliers) of some individual time series caused the model to be poorly estimated for some drug combinations. Therefore, we decided to truncate the data at 8 weeks. Time series corresponding to one of these combinations, encorafenib and LEE011, are shown in Fig. 2.

Mice given Everolimus, BYL719, and BKM120 as monotherapies were not given the drugs with the same dose as in the combination arms, and in these cases, we assumed dose-proportional PK. As a justification for this, Everolimus has been shown to approximately exhibit linear PK (AUC) in mice (Center for Drug Evaluation and Research, 2009). Similar evidence has been seen in rats for the two other drugs (Center for Drug Evaluation and Research, 2018; Novartis, 2016).

The replicates in the preclinical data allow us to evaluate the independent drug action hypothesis in dynamical system modeling. We do this by estimating p along with all other model parameters in the estimation procedure. How well a combination therapy can be described by independent drug action is a function of both the individual efficacy parameters along with p. Therefore, we define,

$$E := \frac{G(a_1, a_2, p)}{\max(a_1, a_2)},$$

as a measure of how well independent drug action describes the combination. A value of E close to one would indicate that independent drug action describes the combination well.

Table 1
Dosing schedule for modeled drug combinations. GC: Gastric Cancer, BC: Breast Cancer, CRC: Colorectal Cancer, CM: Cutaneous Melanoma, PDAC: Pancreatic Ductal Adenocarcinoma, qd: Once a day, q2d: Every second day, qw: once a week, bid: twice a day.

Drug Combination	Cancer Type	N^*	Drug 1 / Drug 2 / Combo (mg/kg)
LEE011 + Everolimus	**GC**	55	180 qd / 20 qd / 180 qd + 10 qd
LJM716 + Trastatuzumab	**BC**	39	25 q2d / 15 qw / 25 q2d + 15 qw
BYL719 + LEE011	**BC**	39	50 qd / 250 qd / 25 qd + 250 qd
BYL719 + LJM716	**BC**	39	50 qd / 25 q2d / 30 qd + 25 q2d
BYL719 + Binimetinib	**CRC**	44	50 qd / 10 bid / 25 qd + 10 bid
LEE011 + Encorafenib	**CM**	33	250 qd / 20 qd / 250 qd + 20 qd
LEE011 + Binimetinib	**CM**	29	250 qd / 10 bid / 250 qd + 10 bid
Binimetinib + BKM120	**PDAC**	37	3.5 bid / 35 qd / 3.5 bid + 30 qd
Binimetinib + Figitumumab	**PDAC**	28	3.5 bid / 20 qw / 3.5 bid + 20 qw

*Average sample size of all treatment arms.

2.3. Computational methods

When calibrating models to preclinical data, we quantify variability between patients by letting a_1, a_2, and k_g in Eq. (1) be lognormally distributed. There is also variability between PDXs created from the same patient's tumor, *i.e.*, inter-occasional variability (IOV) (Laporte-Simitsidis et al., 2000). However, the experimental setup (few individual replicates) made this variability hard to quantify and we therefore only estimate this for TS_0, and fix the standard deviation of k_g to 0.1, which approximately describes the variability in growth rates within cell lines (Wong et al., 2012; Cardilin et al., 2017). IOV was also assumed to be lognormally distributed.

All model parameters were estimated simultaneously, using the Monolix software (Monolix, 2021), for all treatment groups within each drug combination, but each combination was modeled separately. Both a proportional and additive error term was used to describe the

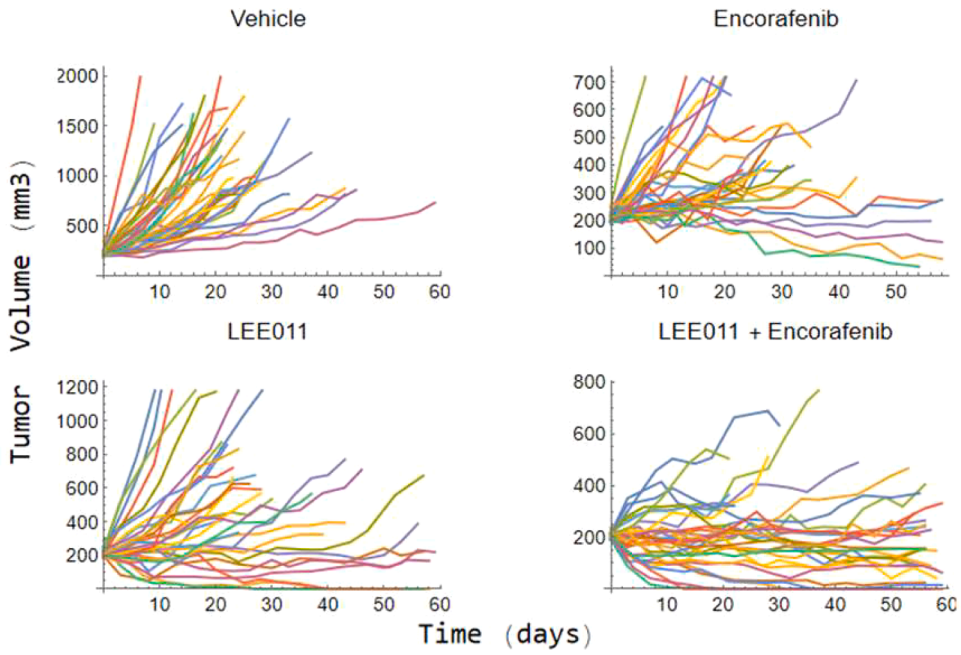

Fig. 2. Illustration of the preclinical data for one of the model combinations: Encorafenib and LEE011.

observation error. The models were primarily validated based on the precision of estimated parameters, individual fits, empirical Bayes estimates (EBEs), and observation *versus* model prediction plots. Mathematica version 13.1 (Monolix, 2022) was used to create all plots shown in the paper.

3. Results

The results section is split into two parts. The analytical results are presented in the first and the modeling results in the second.

3.1. Analysis of the distribution of PFS

Recall that T denotes the PFS time and that it is greater than zero. To find its distribution, we start by integrating the differential equation in Eq. (1), and then inserting the result into Eq. (2), which yields,

$$20 = 100\frac{e^{\int_0^T g(\tau)d\tau} - e^{\int_0^{t_{nadir}} g(\tau)d\tau}}{e^{\int_0^{t_{nadir}} g(\tau)d\tau}}, \qquad (3)$$
$$g(t) = k_g - G(k_1(t), k_2(t), p).$$

Next, we have to solve for T and then evaluate the resulting random variable. However, an explicit expression for the CDF, $F_T(t)$, of this random variable only exists in certain cases. The models we consider contain log-normally distributed parameters, specifically, in the analytical part we assume that $\alpha_i \sim LN(\mu_{a_i}, \sigma_{a_i})$. Therefore, we can only allow certain mathematical operations between the parameters in the model, specifically, we consider addition and the max function. Moreover, exact analytical expressions are not obtained for all models we consider even with this restriction, and we therefore have to resort to some approximations. Finally, we let $\alpha_i\overline{C_i} = a_i \sim LN(\mu_{a_i}, \sigma_{a_i})$, where $\mu_{a_i} = \mu_{\alpha_i} + \log(\overline{C_i})$ and with CDFs denoted by $F_{a_i}(t)$.

We first solve Eq. (3) under the simplification that the resistance is negligible and only a single drug is given. Next, we perform the same analysis but for both an additive combination therapy and under the assumption of independent drug action. Both steps are then repeated for the full model including non-negligible resistance. The CDF of the PFS time for each of these separate scenarios is shown in Table 2. Detailed derivations of the CDFs for all models we consider can be found in the supplementary information.

Table 2
A summary of the CDF of T for all different model assumptions analyzed.

Treatment arm	Resistance	Correlation	Interaction	$F_T(t)$
Mono	No	-	-	$F_{ai}\left(k_g - \frac{\log(1.2)}{t}\right)$
Combo	No	No	Additive	$F_{a3}\left(k_g - \frac{\log(1.2)}{t}\right)$
Combo	No	No	Independent drug action	$F_{a_1}\left(k_g - \frac{\log(1.2)}{t}\right) F_{a_2}\left(k_g - \frac{\log(1.2)}{t}\right)$
Combo	No	Yes	Independent drug action	$F_A\left(k_g - \frac{\log(1.2)}{t}\right)$
Mono	Yes	-	-	$w_i\, F_{L_i}(t) + (1 - w_i)F_{N_i}(t)$
Combo	Yes ($\gamma_1 = \gamma_2$)	No	Additive	$w_3\, F_{LN_3}(t) + (1 - w_3)F_{N_3}(t)$
Combo	Yes ($\gamma_1 \neq \gamma_2$)	No	Additive	Non-analytical
Combo	Yes ($\gamma_1 = \gamma_2$)	No	Independent drug action	$w_1\, w_2\, F_{L_1}(t)F_{L_2}(t) + w_1(1 - w_2)F_{N_2}(t) + (1 - w_1)w_2F_{N_1}(t) + (1 - w_1)(1 - w_2)F_{N_1}(t)F_{N_2}(t)$
Combo	Yes ($\gamma_1 = \gamma_2$)	Yes	Independent drug action	$w_{s_1}\, F_{ML}(t) + w_{s_2}\, F_{CN_2}(t) + w_{s_3}\, F_{CN_1}(t) + w_{s_4}\, F_{MN}(t)$
Combo	Yes ($\gamma_1 \neq \gamma_2$)	Yes	Independent drug action	Non-analytical

3.2. Negligible resistance

3.2.1. Monotherapy

If we consider the monotherapy case with no resistance, *i.e.*, $\gamma_i = 0$ and $g(t) = k_g - a_i$, then the CDF of T can be written as,

$$F_T(t) = F_{ai}\left(k_g - \frac{\log(1.2)}{t}\right).$$

Hence, the PFS time does not follow a named distribution but can be expressed with the help of the lognormal CDF. A histogram and the survival curve from model simulations are shown in Fig. 3.

3.2.2. Additive combination therapy

The combined efficacy of an uncorrelated additive two drug combination therapy ($p = 1$) can be approximated as a lognormally distributed random variable using the Fenton-Wilkinsson approximation (see supplementary information) (Cobb et al., 2012). Hence, the PFS for patients given such a combination therapy will approximately follow the same type of distribution as in the monotherapy case, but with different parameters. Consequently, the CDF is given by,

$$F_T(t) \approx F_{a3}\left(k_g - \frac{\log(1.2)}{t}\right),$$

where $a_3 \sim LN(\mu_{a_3}, \sigma_{a_3})$ is the approximated sum of a_1 and a_2 with μ_{a3} and σ_{a_3} given by,

$$\mu_{a_3} = \log\left(\sum_{i=1}^{2} e^{\mu_i + \frac{\sigma_i^2}{2}}\right) - \frac{\sigma_3^2}{2}, \tag{4}$$

$$\sigma_{a_3} = \sqrt{\log\left(\frac{\sum_{i=1}^{2} e^{2\,\mu_i + \sigma_i^2}\left(e^{\sigma_i^2} - 1\right)}{\left(\sum_{i=1}^{2} e^{\mu_i + \frac{\sigma_i^2}{2}}\right)^2} + 1\right)}. \tag{5}$$

3.2.3. Independent drug action combination therapy

In the case of independent drug action ($p = \infty$), the CDF of T is given by,

$$F_T(t) = F_A\left(k_g - \frac{\log(1.2)}{t}\right),$$

respectively. Here $A = \max(a_1, a_2)$ and $F_A(t)$ is the CDF of this random variable.

Uncorrelation implies independence for lognormally distributed random variables. Hence, if the potency parameters are uncorrelated the CDF is reduced to,

$$F_T(t) = F_{a_1}\left(k_g - \frac{\log(1.2)}{t}\right) F_{a_2}\left(k_g - \frac{\log(1.2)}{t}\right),$$

3.3. Non-Negligible resistance

3.3.1. Monotherapy

We now consider the case with resistance and again start with the monotherapy case. The CDF of T can, under certain conditions, be approximated by,

$$\begin{aligned} F_T(t) &= w_i P(T < t | a_i < k_g) + (1 - w_i) P(T < t | a_i > k_g) \\ &\approx w_i F_{L_i}(t) + (1 - w_i) F_{N_i}(t), \end{aligned}$$

where $w_i = P(a_i \le k_g)$. This is a mixture of a truncated shifted lognormal distribution (F_{L_i}) with parameters $\mu = \mu_{a_i} - \log(\gamma_i\, k_g)$, $\sigma = \sigma_{a_i}$, and shift parameter, $\theta = \frac{\log(1.2)}{k_g}$, and a truncated normal distribution (F_{N_i}) with parameters $\mu = \frac{\log(1.2)}{k_g} + \frac{\mu_{ai}}{\gamma_i} + \frac{(1 - \log(k_g))}{\gamma_i}$ and $\sigma = \frac{\sigma_{a_i}}{\gamma_i}$. Both are truncated at $t = \frac{\log(1.2)}{k_g} + \frac{1}{\gamma_i}$. For more information regarding shifted lognormal distributions, see supplementary information. The PDF of the mixture distribution together with a histogram of simulated PFS times is shown in Fig. 4.

3.3.2. Additive combination therapy

An analytical expression for the CDF of T is not available for the case of an additive combination therapy when $\gamma_1 \neq \gamma_2$. Figure S2 shows two comparisons between the histograms of simulated PFS times under the assumption that $\gamma_1 = \gamma_2$ and two choices of $\gamma_1 \neq \gamma_2$.

However, if we assume $\gamma_1 = \gamma_2$, we can use the same argument as in the additive no-resistance case, and hence, the CDF can be approximated as

$$\begin{aligned} F_T(t) &\approx w_3\, F_{LN_3}(t) + (1 - w_3) F_{N_3}(t), \\ w_3 &= P(a_3 \le k_g). \end{aligned}$$

where $a_3 \sim LN(\mu_{a_3}, \sigma_{a_3})$ is the approximated sum of a_1 and a_2 with μ_{a3} and σ_{a_3} given by Eqs. (4) and (5). Figure S3 shows that this approach approximates the full model well for the used parameters.

3.3.3. Independent drug action combination therapy

For independent drug action ($p = \infty$), we start by assuming that $\gamma_1 = \gamma_2 = \gamma$. Later on, we also consider $\gamma_1 \neq \gamma_2$. If a_1 and a_2 are uncorrelated

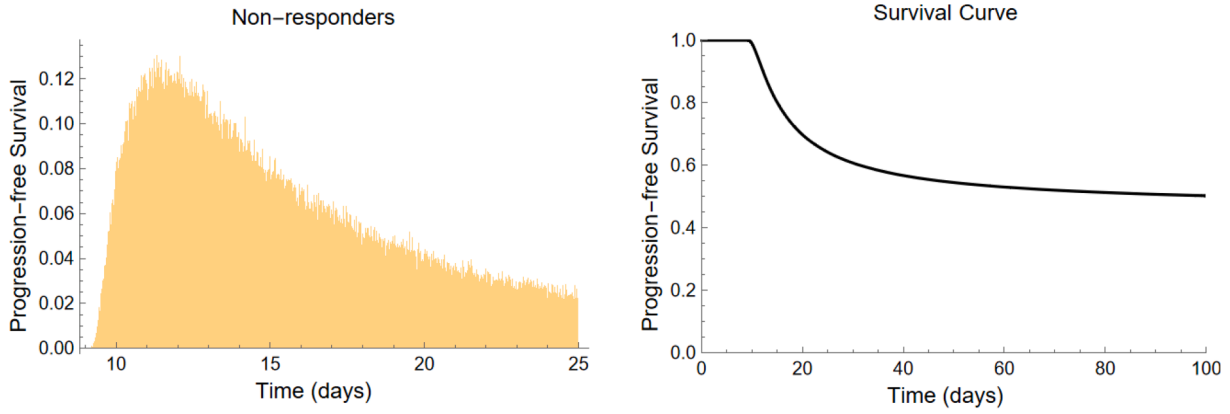

Fig. 3. (Left) Simulated histogram of progression-free survival times and corresponding survival curve (right). The parameters used were, $k_g = 0.02\ days^{-1}$, $\mu_{a_i} = -4$, and $\sigma_{ai} = 1$.

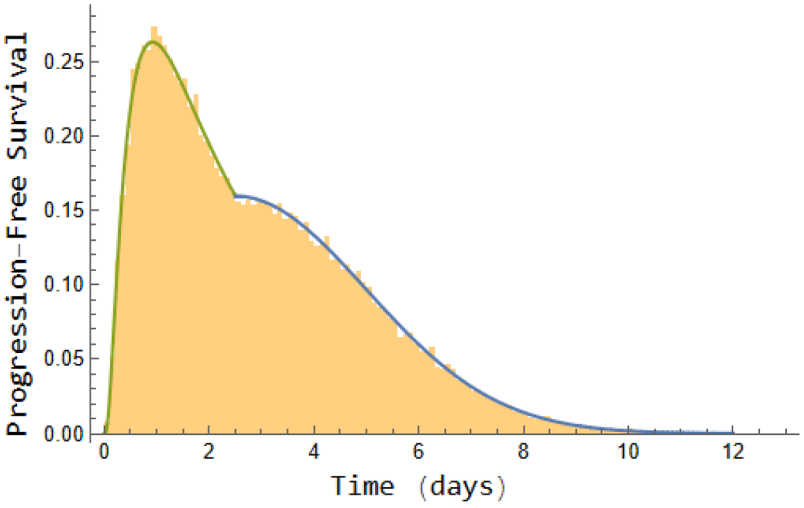

Fig. 4. Histogram of simulated PFS for an exponentially decaying monotherapy and theoretical PDF of lognormal (green) and normal (blue) mixture. The parameters used were, $\gamma_i = 0.4\ days^{-1}$, $k_g = 0.02\ days^{-1}$, $\mu_{a_i} = -4$, $\sigma_{ai} = 1$, and $TS_0 = 100\ mm$.

the CDF of T can be approximated as,

$$F_T(t) \approx w_1 w_2 F_{L_1}(t) F_{L_2}(t) + w_1(1-w_2) F_{L_1}(t) F_{N_2}(t) + (1-w_1) w_2 F_{N_1}(t) F_{L_2}(t) + (1-w_1)(1-w_2) F_{N_1}(t) F_{N_2}(t).$$

For the correlated case, we have,

$$F_T(t) \approx w_{s_1} F_{ML}(t) + w_{s_2} F_{CN_2}(t) + w_{s_3} F_{CN_1}(t) + w_{s_4} F_{MN}(t),$$

where F_{ML} is a truncated log-multinormal distribution, F_{CN_1} and F_{CN_2} are truncated conditional multivariate normal distributions, and F_{MN} is a truncated multivariate normal distribution. Furthermore, the weights of the mixture are,

$$w_{s_1} = P(k_g \geq a_1, k_g \geq a_2),$$

$$w_{s_2} = P(k_g \geq a_1, k_g < a_2),$$

$$w_{s_3} = P(k_g < a_1, k_g \geq a_2),$$

$$w_{s_4} = P(k_g < a_1, k_g < a_2).$$

If we assume that $\gamma_1 \neq \gamma_2$ we will end up with a similar expression for the CDF, however, most of the individual mixture components will be mixture distributions themselves, with non-analytical expressions. Figure S4 shows two comparisons between the histograms of simulated PFS times under the assumption that $\gamma_1 = \gamma_2$ and two choices of $\gamma_1 \neq \gamma_2$.

3.4. *Simulation-based* analysis

3.4.1. *Preclinical modeling*

Estimated parameters and E values of each drug combination are shown in Table 3. Here, a_1 and a_2 refer to the drug kill rate parameter of the first and second, drug, respectively, in the combination. The estimated growth rate parameters varied between 0.04 and 0.07 1/days. From this, a tumor doubling time of between 10 and 17 days was estimated. The exponent p was estimated to be between 0.8 and 180.

Fig. 5 shows tumor volume model predictions against observed data for all individuals for all treatment arms. Kaplan-Meier VPCs are shown in Fig. 6 for one combination of each type of interaction (LJM716 + Trastuzumab: Independent drug action, LEE011 + encorafenib: additive/slightly antagonistic, and BYL719 + LEE011: Synergism).

3.4.2. *Clinical PFS simulations*

To compare the analytical results with a real-world scenario, we made simulations using the clinical PFS model. The results from these simulations are shown in Fig. 7. The left of the figure shows a histogram of all individuals together, whereas in the right part the population is split into non-responders ($t_{nadir} = 0$) and responders ($t_{nadir} \neq 0$).

4. Discussion

Studies that explore model-based translation of preclinical results to the clinic often focus on quantitative differences (Yates and Fairman,

Table 3
Estimated values for the efficacy parameter a_i of each drug along with the estimated p for each combination and the resulting E. GC: Gastric Cancer, BC: Breast Cancer, CRC: Colorectal Cancer, CM: Cutaneous Melanoma, PDAC: Pancreatic ductal adenocarcinoma. RSE: Relative Standard Error.

Drug Combination	Cancer type	TS_0 (RSE %)	k_g (RSE %)	a_1 (RSE %)	a_2 (RSE %)	p (RSE %)	E	Interaction
LEE011 + Everolimus	**GC**	250 (2)	0.04 (7)	0.015 (16)	0.023 (9)	1.6 (2)	1.3	Antagonistic
LJM716 + Trastuzumab	**BC**	230 (3)	0.05 (8)	0.01 (32)	0.003 (49)	141 (0.2)	1	Independent drug action
BYL719 + LEE011	**BC**	240 (2)	0.05 (9)	0.022 (19)	0.024 (11)	0.8 (2)	2.3	Synergistic
BYL719 + LJM716	**BC**	220 (2)	0.05 (8)	0.027 (14)	0.01(34)	2.6 (6)	1	Independent drug action
BYL719 + Binimetinib	**CRC**	220 (2)	0.04 (8)	0.015 (14)	0.025(11)	0.8 (1)	1.89	Synergistic
LEE011 + Encorafenib	**CM**	220 (2)	0.07 (9)	0.05 (10)	0.012 (25)	1.1 (0.3)	1.9	Additive*
LEE011 + Binimetinib	**CM**	210 (2)	0.07 (8)	0.04 (13)	0.04 (10)	1.1 (0.3)	1.9	Additive*
Binimetinib + BKM120	**PDAC**	260 (2)	0.04 (9)	0.02 (11)	0.02 (13)	1 (0.2)	2	Additive
Binimetinib + Figitumumab	**PDAC**	270 (2)	0.04 (7)	0.02 (20)	0.001 (84)	180 (0.03)	1	Independent drug action

* Additive/slightly antagonistic.

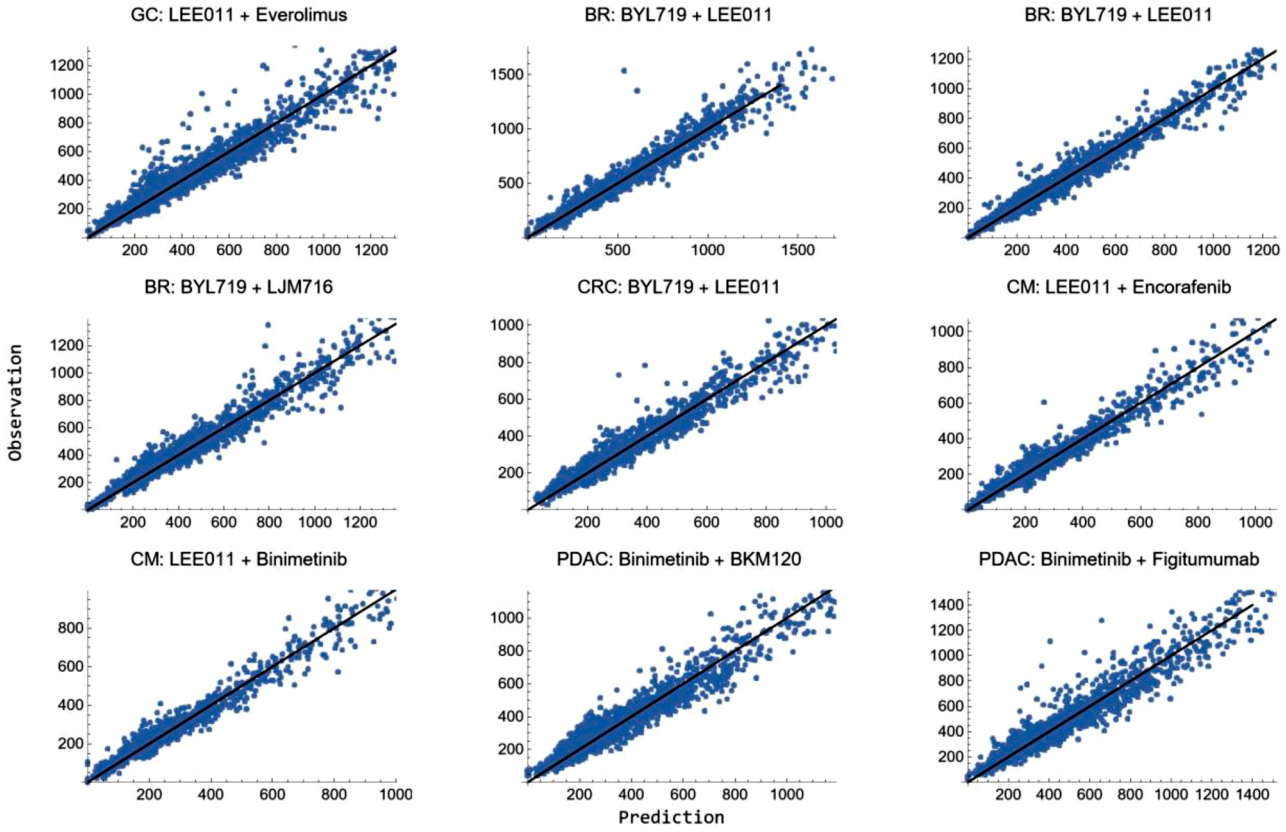

Fig. 5. Longitudinal tumor volume model prediction plotted against observed data for each drug combination.

2022). For example, the correlation between reduction in tumor size (tumor growth inhibition in %) and the overall response rate has been investigated for several different drugs (Wong et al., 2012). Building upon this, we have also in a previous study estimated how different preclinical model parameters should be scaled for the model predictions to line up with clinical data (Baaz et al., 2022). However, in this paper, we also show that there are important qualitative differences stemming from the choice of preclinical and clinical models.

The Claret model includes the feature of exponentially decaying drug effects due to acquired resistance (Claret et al., 2009; Yu et al., 2020). However, for preclinical data, the resistance term has in many cases been shown to be superfluous (Zwep et al., 2021). It has been shown that the probability of developing drug resistance increases with the drug dose, and, thus, an important reason for this discrepancy can simply be that the preclinical doses are too low in comparison with the clinical doses (Martin et al., 2018; Tomasetti, 2012). Another factor could be the difference in length between clinical and preclinical trials.

We show in this paper that because of the removal of the resistance term in the preclinical model, the distribution of PFS changes compared to the clinical model. For example, in the case of monotherapies, the preclinical (model without resistance) PFS time follows an unnamed distribution, whose CDF can be expressed using a lognormal distribution, whereas in the clinical case, (model with resistance), it follows a mixture of a lognormal and normal distribution under certain conditions. When these conditions are not fulfilled the clinical CDF still differs from the preclinical but is intractable.

Moreover, when considering combination therapies, assuming equal resistance rate parameters allows for a fairly straightforward extension of the monotherapy cases. Without this assumption, the distributions become more complicated and lack analytical CDFs. However, for the parameters we used, our simulations show that these distributions are relatively similar to the equal resistance cases.

To arrive at these analytical results, we have had to make several assumptions. Our approach has been to make reasonable assumptions to arrive at well-known distributions and then generalize the results using simulations to show that the qualitative nature of the results still holds. For example, Fig. 7 shows the distribution of PFS from a previously calibrated clinical model where four parameters were assumed to follow a lognormal distribution. In the left part of the figure, we can see that the histogram of simulations of T resembles a lognormal distribution but for the fact that there are two peaks. This hints at an underlying mixture distribution, which can be seen to be the case in the right part of the figure where histograms from the same simulation are shown but with responders and non-responders separated. Hence, we can conclude that the qualitative differences that our theoretical results show for the simplified model also hold for more complex models. Moreover, since the survival function of PFS is simply the proportion of patients that have been classified as Progressive Diseases at different time points, the same conclusions can be drawn if the analysis, *mutatis mutandis*, is performed for the overall response rate instead. Thus, this could be an important factor to take into consideration when making model-based translational predictions of both PFS and overall response rates. We also want to reiterate that this analysis is performed for PFS stemming from target progression. In a real clinical setting, PFS is also set by non-target progression *e.g.,* if new lesions appear (Eisenhauer et al., 2009; Yu et al., 2020). Moreover, censoring due to random dropout is not considered either. Incorporating both types of events should decrease the PFS time for the population. A potential next step could be to extend the analysis to encompass these two types of events as well.

The reason for the mixture distribution comes from the fact that the definition of target progression uses the nadir SLD as a reference point and whether the nadir occurs at the start of the trial or later, will affect the equations. Thus, for the Claret model with any distribution on any parameter, any treatment schedule, and with any biologically reasonable parameter values, the PFS time will follow a mixture distribution. Analytical expressions for the individual components of the mixture are

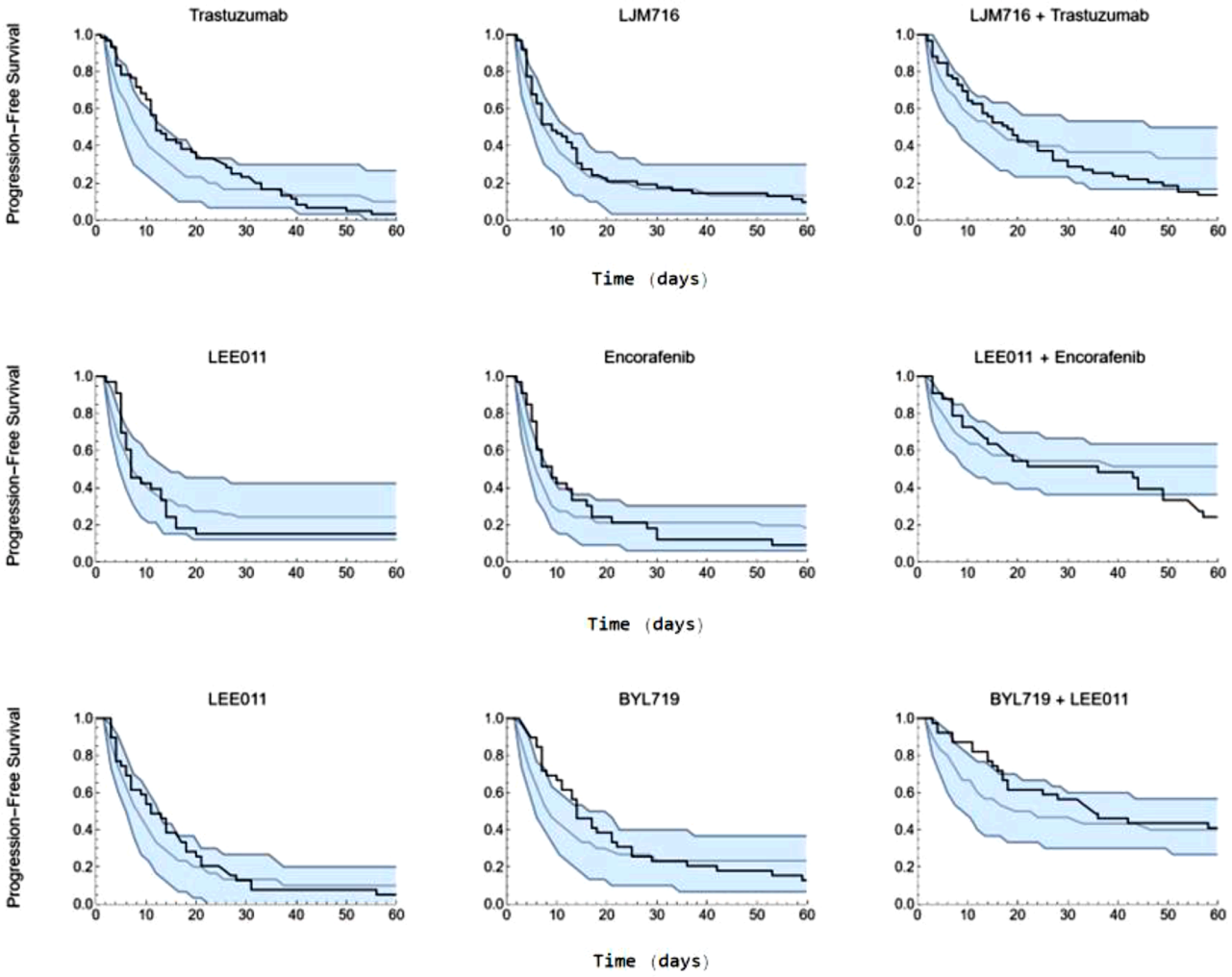

Fig. 6. Kaplan-Meier VPCs for PFS. The black line is the PFS estimated from the data, grey is the median PFS prediction from the model and the blue area is a 95 % confidence interval.

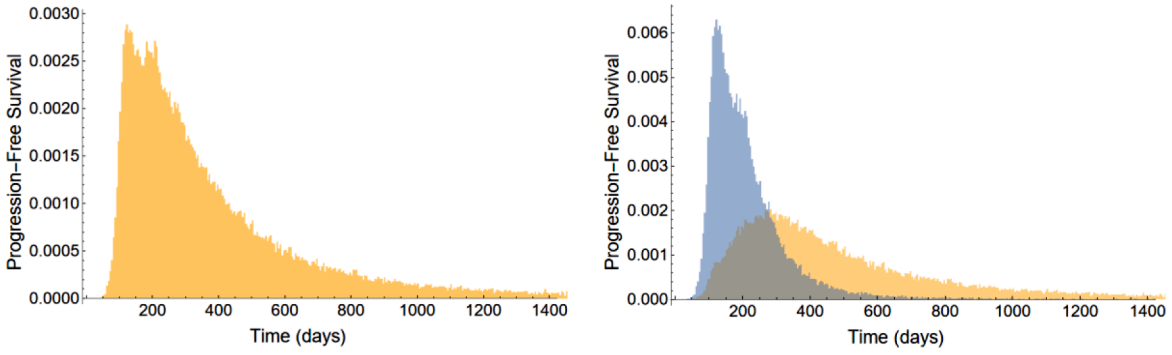

Fig. 7. (Left) Histogram of simulated PFS based on target progression using a previous model that was calibrated with clinical data (Baaz et al., 2023). (Right) Histograms of simulated PFS using the same model but with individuals being separated based on if $t_{nadir} = 0$ (yellow) or $t_{nadir} \neq 0$ (blue).

in many cases impossible to find but, as we have shown, can be simulated.

From this analysis, we have shown that there exist differences in predictions of PFS, but what this implies is not entirely clear. For example, how much of the discrepancies between predictions based on preclinical modeling, and clinical results, that these qualitative differences can explain is something that needs to be further studied. One idea for further study could be to calibrate a model using preclinical data and then translate the model using *e.g.,* allometric scaling or replacement of animal parameters with human parameters. The translated model could then be used to make clinical predictions and a comparison could be performed between predictions with these qualitative differences accounted for and not accounted for.

Figs. 5 and 6 show that the preclinical TGI model is able to capture the observed time series and PFS of the PDXs fairly well. Minor discrepancies can be observed for the monotherapies at the end of the PFS

predictions, but this is most likely due to not taking dropout into consideration and we note that the observations are still more or less covered by the confidence intervals. The only two parameter estimates with somewhat high RSE were the potency parameters for figitumumab and trastuzumab and the reason for this is most likely their poor efficacy. It has previously been shown that many PFS curves for PDXs given different combination therapies were consistent with independent drug action (Palmer and Sorger, 2017). Since they also only considered target progression in the cited paper, the same should be true if the analysis is performed using dynamical systems modeling and model-based PFS predictions. We found that four of the nine combinations were consistent with independent-drug action and five surpassed it. These same five combinations were also found to outperform independent drug action in the previous study. Thus, our findings align well with what previously has been observed.

5. Conclusions

By deriving the probability distribution of PFS for both a widely used clinical model and a preclinical model we have shown discernible quantitative differences in the PFS predictions stemming from these two models. This was done for both monotherapies and combination therapies under different assumptions of combination therapy efficacy. The results naturally apply to other metrics based on the RECIST criteria such as response rates. These differences should be carefully considered when performing inter-species translation.

Furthermore, we modeled experimental preclinical data and used a previously calibrated clinical model to show that the above-mentioned conclusions also hold when applying our findings to real-world patient populations. Additionally, we demonstrated that independent-drug action can effectively describe the tumor dynamics of PDXs given certain drug combinations.

Funding

Marcus Baaz was supported by an educational research grant from Merck KGaA, Darmstadt, Germany (CrossRef Funder ID: 10.13039/100009945).

CRediT authorship contribution statement

Marcus Baaz: Writing – review & editing, Writing – original draft, Visualization, Validation, Methodology, Investigation, Formal analysis, Data curation, Conceptualization. **Tim Cardilin:** Writing – review & editing, Validation, Supervision, Methodology, Investigation, Formal analysis, Conceptualization. **Mats Jirstrand:** Writing – review & editing, Validation, Supervision, Project administration, Methodology, Investigation, Funding acquisition, Formal analysis.

Declaration of Interest

The authors declared no competing interests for this work.

Data availability

All data is publicly available.

Supplementary materials

Supplementary material associated with this article can be found, in the online version, at doi:10.1016/j.ejps.2024.106901.

References

Arrowsmith, J., Miller, P., 2013. Phase II and phase III attrition rates 2011–2012. Nat. Rev. Drug Discov. 12, 569. https://doi.org/10.1038/nrd4090.
Baaz, M., Cardilin, T., Jirstrand, M., 2023. Model-based prediction of progression-free survival for combination therapies in oncology. CPT Pharmacomet. Syst. Pharmacol. https://doi.org/10.1002/psp4.13003.
Baaz, M., Cardilin, T., Jirstrand, M., 2023. Model-based prediction of progression-free survival for combination therapies in oncology. CPT Pharmacomet. Syst. Pharmacol. 12, 1227–1237. https://doi.org/10.1002/psp4.13003.
Baaz, M., Cardilin, T., Lignet, F., Jirstrand, M., 2022. Optimized scaling of translational factors in oncology: from xenografts to RECIST. Cancer Chemother. Pharmacol. 90, 239–250. https://doi.org/10.1007/s00280-022-04458-8.
Cardilin, T., Almquist, J., Jirstrand, M., Sostelly, A., Amendt, C., El Bawab, S., et al., 2017. Tumor static concentration curves in combination therapy. AAPS J. 19, 456–467. https://doi.org/10.1208/s12248-016-9991-1.
Center for Drug Evaluation and Research. Pharmacology Review of Afinitor (everolimus) 2009.
Center for Drug Evaluation and Research. Pharmacology Review of Alpelisib 2018.
Claret, L., Girard, P., Hoff, P.M., Van Cutsem, E., Zuideveld, K.P., Jorga, K., et al., 2009. Model-based prediction of phase III overall survival in colorectal cancer on the basis of phase II tumor dynamics. J. Clin. Oncol. 27, 4103–4108. https://doi.org/10.1200/JCO.2008.21.0807.
Cobb, B., Rumí, R., Salmerón, A., 2012. Approximating the distribution of a sum of log-normal random variables. In: Proc. 6th Eur. Workshop Probabilistic Graph. Models PGM 2012.
Douillard, J.-Y., Oliner, K.S., Siena, S., Tabernero, J., Burkes, R., Barugel, M., et al., 2013. Panitumumab–FOLFOX4 treatment and RAS mutations in colorectal cancer. N. Engl. J. Med. 369, 1023–1034. https://doi.org/10.1056/NEJMoa1305275.
Eisenhauer, E.A., Therasse, P., Bogaerts, J., Schwartz, L.H., Sargent, D., Ford, R., et al., 2009. New response evaluation criteria in solid tumours: revised RECIST guideline (Version 1.1). Eur. J. Cancer 45, 228–247. https://doi.org/10.1016/j.ejca.2008.10.026.
Fitzgerald, J.B., Schoeberl, B., Nielsen, U.B., Sorger, P.K., 2006. Systems biology and combination therapy in the quest for clinical efficacy. Nat. Chem. Biol. 2, 458–466. https://doi.org/10.1038/nchembio817.
Gao, H., Korn, J.M., Ferretti, S., Monahan, J.E., Wang, Y., Singh, M., et al., 2015. High-throughput screening using patient-derived tumor xenografts to predict clinical trial drug response. Nat. Med. 21, 1318–1325. https://doi.org/10.1038/nm.3954.
Gutman, S.I., Piper, M., Grant, M.D., Basch, E., Oliansky, D.M., Aronson, N., 2013. Background. Agency for Healthcare Research and Quality (US).
Koga, Y., Ochiai, A., 2019. Systematic review of patient-derived xenograft models for preclinical studies of anti-cancer drugs in solid tumors. Cells 8, 418. https://doi.org/10.3390/cells8050418.
Laporte-Simitsidis, S., Girard, P., Mismetti, P., Chabaud, S., Decousus, H., Boissel, J.-P., 2000. Inter-study variability in population pharmacokinetic meta-analysis: when and how to estimate It? J. Pharm. Sci. 89, 155–167. https://doi.org/10.1002/(SICI)1520-6017(200002)89:2<155::AID-JPS3>3.0.CO;2-2.
Leander, J., Almquist, J., Johnning, A., Larsson, J., Jirstrand, M., 2021. Nonlinear mixed effects modeling of deterministic and stochastic dynamical systems in wolfram mathematica. IFAC-Pap 54, 409–414. https://doi.org/10.1016/j.ifacol.2021.08.394.
Mak, I.W., Evaniew, N., Ghert, M., 2014. Lost in translation: animal models and clinical trials in cancer treatment. Am. J. Transl. Res. 6, 114–118.
Martin, E.C., Aarons, L., Yates, J.W.T., 2018. Pharmacodynamic modelling of resistance to epidermal growth factor receptor inhibition in brain metastasis mouse models. Cancer Chemother. Pharmacol. 82, 669–675. https://doi.org/10.1007/s00280-018-3630-8.
Mohamed, A.F., Kristoffersson, A.N., Karvanen, M., Nielsen, E.I., Cars, O., Friberg, L.E., 2016. Dynamic interaction of colistin and meropenem on a WT and a resistant strain of Pseudomonas aeruginosa as quantified in a PK/PD model. J. Antimicrob. Chemother 71, 1279–1290. https://doi.org/10.1093/jac/dkv488.
Mohs, R.C., Greig, N.H., 2017. Drug discovery and development: role of basic biological research. Alzheimers Dement. Transl. Res. Clin. Interv. 3, 651–657. https://doi.org/10.1016/j.trci.2017.10.005.
Mokhtari, R.B., Homayouni, T.S., Baluch, N., Morgatskaya, E., Kumar, S., Das, B., et al., 2017. Combination therapy in combating cancer. Oncotarget 8, 38022–38043. https://doi.org/10.18632/oncotarget.16723.
Monolix 2021 R2, Lixoft SAS, a Simulations Plus company Lixoft SAS, a Simulations Plus company.
Wolfram Research, Inc. Mathematica 2022.
Novartis. Buparlisib (BKM120): Protocol CBKM120H2201 /NCT01852292 2016.
Palmer, A.C., Sorger, P.K., 2017. Combination cancer therapy can confer benefit via patient-to-patient variability without drug additivity or synergy. Cell 171, 1678–1691.e13. https://doi.org/10.1016/j.cell.2017.11.009.
Plana, D., Palmer, A.C., Sorger, P.K., 2022. Independent drug action in combination therapy: implications for precision oncology. Cancer Discov. 12, 606–624. https://doi.org/10.1158/2159-8290.CD-21-0212.
Pomeroy, A.E., Schmidt, E.V., Sorger, P.K., Palmer, A.C., 2022. Drug independence and the curability of cancer by combination chemotherapy. Trends. Cancer 8, 915–929. https://doi.org/10.1016/j.trecan.2022.06.009.
Seyhan, A.A., 2019. Lost in translation: the valley of death across preclinical and clinical divide – identification of problems and overcoming obstacles. Transl. Med. Commun. 4, 18. https://doi.org/10.1186/s41231-019-0050-7.
Slater, H.C., Okell, L.C., Ghani, A.C., 2017. Mathematical Modelling to Guide Drug Development for Malaria Elimination. Trends. Parasitol. 33, 175–184. https://doi.org/10.1016/j.pt.2016.09.004.

Tomasetti, C., 2012. On the probability of random genetic mutations for various types of tumor growth. Bull. Math. Biol. 74 https://doi.org/10.1007/s11538-012-9717-1, 10.1007/s11538-012-9717–1.

Vakil, V., Trappe, W., 2019. Drug combinations: mathematical modeling and networking methods. Pharmaceutics 11, 208. https://doi.org/10.3390/pharmaceutics11050208.

Wong, H., Choo, E.F., Alicke, B., Ding, X., La, H., McNamara, E., et al., 2012. Antitumor activity of targeted and cytotoxic agents in murine subcutaneous tumor models correlates with clinical response. Clin. Cancer Res. 18, 3846–3855. https://doi.org/10.1158/1078-0432.CCR-12-0738.

Wu, J., 2010. Statistical inference for tumor growth inhibition T/C ratio. J. Biopharm. Stat. 20, 954–964. https://doi.org/10.1080/10543401003618983.

Yates, J.W.T., Fairman, D.A., 2022. How translational modeling in oncology needs to get the mechanism just right. Clin. Transl. Sci. 15, 588–600. https://doi.org/10.1111/cts.13183.

Yu, J., Wang, N., Kågedal, M., 2020. A new method to model and predict progression free survival based on tumor growth dynamics. CPT Pharmacomet. Syst. Pharmacol. 9, 177–184. https://doi.org/10.1002/psp4.12499.

Zhuang, S.H., Xiu, L., Elsayed, Y.A., 2009. Overall survival: a gold standard in search of a surrogate: the value of progression-free survival and time to progression as end points of drug efficacy. Cancer J. 15, 395–400. https://doi.org/10.1097/PPO.0b013e3181be231d.

Zwep, L.B., Duisters, K.L.W., Jansen, M., Guo, T., Meulman, J.J., Upadhyay, P.J., et al., 2021. Identification of high-dimensional omics-derived predictors for tumor growth dynamics using machine learning and pharmacometric modeling. CPT Pharmacomet. Syst. Pharmacol. 10, 350–361. https://doi.org/10.1002/psp4.12603.